Shap. Mem. Superelasticity
https://doi.org/10.1007/s40830-024-00484-y

REVIEW

SMA Film-Based Elastocaloric Cooling Devices

Jingyuan Xu[1] · Florian Bruederlin[1] · Lars Bumke[2] · Hinnerk Ossmer[1] · Eckhard Quandt[2] · Shuichi Miyazaki[3] · Manfred Kohl[1]

Received: 11 January 2024 / Revised: 1 March 2024 / Accepted: 1 March 2024

Abstract The ongoing trend of miniaturization and increasing power density in miniaturized systems demand for active temperature control and cooling. The cooling technologies utilized today depend on environmentally harmful substances or are bound to low efficiencies. This leads to an urgent need for innovative cooling technologies that are both environmentally friendly and efficient. This report focuses on shape memory alloy (SMA) film-based elastocaloric (eC) cooling, as SMA films exhibit a large eC effect and enable efficient heat transfer through solid-to-solid contact due to their large surface-to-volume ratio. Among the different material candidates, TiNiCuCo films are of special interest due to their ultra-low fatigue properties and small hysteresis. Single-stage SMA film-based eC devices reach a device temperature span up to 14 K combined with a high specific cooling capacity of up to 19 W g^{-1}. However, absolute cooling capacities in the small-scale device are limited to 220 mW and the device temperature span already reaches the adiabatic limit of the used SMA film. To overcome the limitations in cooling capacity and device temperature span, novel advanced device architectures are explored. A parallelized cooling device combining the eC effect of five SMA films is engineered to increase the absolute cooling capacity up to 900 mW, while it preserves the high specific cooling capacity unique to SMA film-based cooling devices. A cascaded eC cooling device is developed, which consists of a serial arrangement of three SMA films. In this case, the device temperature span is increased beyond the adiabatic limit of a single film to 27.3 K. These results provide a basis for next-generation SMA film-based eC cooling technology.

Keywords Elastocaloric cooling · Shape memory alloy films · Caloric cooling

Introduction

Presently, approximately 3 billion devices are currently deployed for cooling applications, encompassing household, commercial, and transport refrigeration, as well as air conditioning systems and heat pumps. These collectively contribute to 17% of the world's total electricity consumption [1]. While vapor-compression cooling dominates the market for macro-scale cooling provision, utilizing a technology that has been in existence for two centuries, it relies on volatile gaseous refrigerants with a significant global warming potential (GWP). Addressing the cooling needs of miniature-scale devices is primarily achieved through thermoelectric coolers. However, these coolers operate with low energy efficiency [2]. Consequently, there is an urgent demand for innovative cooling technologies that prioritize both environmental sustainability and high efficiency.

A promising alternative is solid-state cooling based on stress-induced thermal changes in superelastic shape memory alloys (SMA), i.e., elastocaloric cooling (eC), which exhibits zero environmental impact due to the absence of refrigerant leakage (i.e., zero-GWP) and a high material

This invited article is part of a special topical focus in *Shape Memory and Superelasticity* on Elastocaloric Effects in Shape Memory Alloys. The issue was organized by Stefan Seelecke and Paul Motzki, Saarland University.

✉ Jingyuan Xu
jingyuan.xu@kit.edu

[1] Institute of Microstructure Technology, Karlsruhe Institute of Technology (KIT), Karlsruhe, Germany

[2] Inorganic Functional Materials, Institute for Materials Science, Kiel University, Kiel, Germany

[3] Division of Materials Science, University of Tsukuba, Tsukuba, Japan

Published online: 20 May 2024

efficiency approaching the thermodynamic maximum limit [3]. Superelastic SMAs exhibit an exceptional eC effect. For instance, in NiTi-based SMAs, elastocaloric temperature changes can reach up to 30 K [4], and the associated latent heats can extend to as much as 30 J g^{-1} [5]. eC technology demonstrates a more favorable scaling behavior compared to conventional technologies, making it versatile for both miniaturized systems and macroscopic applications [6, 7].

In the domain of macro-scale cooling applications, research is predominantly directed towards bulk SMA geometry, encompassing SMA tubes [8, 9], plates [10, 11], and wires [12, 13]. Successful eC prototypes employ cascading multiple single-stage schemes [13] and an active regeneration scheme [13, 14]. These strategies enhance the temperature span across devices, addressing the limitations posed by adiabatic temperature changes in SMAs. Validation of cascading multiple single-stage schemes has been achieved through experiments with a three-stage device, showcasing a 28.3 K temperature span [13]. Similarly, active regeneration has proven effective in macro-scale eC devices, initially achieving temperature spans approaching 15 K [13] and subsequently expanding to 31.3 K [9], and demonstrating a cooling power of 260 W [15]. Further enhancement of specific heat transfer areas, achieved through a tubular NiTi regenerator with a spiral cross-section, has resulted in a temperature span of 50.6 K [14]. Despite these advancements, a major drawback of bulk SMA implementation is its low operational frequency, typically less than 1 Hz, limiting specific cooling capacity due to slower heat transfer rates. To mitigate this issue, one proposed heat transfer improvement concept involves the utilization of a fluid's evaporation and condensation processes [16, 17]. Additionally, the requirement for large hydraulic facilities as well as hysteresis characteristic of NiTi SMAs [18] often result in a lower overall coefficient of performance (COP).

SMA films are particularly promising for miniature-scale cooling, as they combine an extraordinary eC effect size and highly efficient heat transfer due to the large surface-to-volume ratio of film geometries. The specific cooling capacity of film-based eC devices could be an order of magnitude larger than that of bulk SMA geometries. This suggests that film-based eC cooling holds significant potential for thermal management in miniature-scale applications, including, but not limited to, microelectronics, aerospace, biomedical applications such as cooling of biological tissue [19], and chemical analytics, e.g., temperature stabilization of lab-on-chip systems [20]. Unlike macro-scale eC devices that use liquid heat transfer fluids to manage heat flow from SMA, the separation of SMA heat flow for film-based eC is achieved through solid-to-solid heat transfer contact between the film and the heat sink/source surfaces.

In this work, we will present the state-of-the-art in SMA film-based eC cooling. We will concentrate on the following TiNi-based films: magnetron-sputtered binary TiNi and Ti–rich TiNiCuCo films as well as cold-rolled TiNiFe foils. Single-stage eC devices with a single SMA film will serve as a benchmark of eC cooling performance. This performance will be compared with advanced eC system architectures, including parallelized and cascaded systems, to point out possible routes for overcoming their limitations in cooling capacity and device temperature span.

Material Properties of SMA Films

TiNi Films

Binary $Ti_{49.6}Ni_{50.4}$ films of 20 µm thickness are fabricated through DC magnetron sputtering. As the as deposited films possess an amorphous crystal structure, the films are crystallized by a two-step heat treatment at 650 °C for 10 min, followed by a further stage at 450 °C for another 10 min.

Figure 1 illustrates the thermal–mechanical performance of the $Ti_{49.6}Ni_{50.4}$ film sample. A cyclic tensile test was conducted at a strain rate of 0.02 s^{-1} on an as-produced sample. The stress–strain characteristics for the first, second, third, and 20th cycles are depicted in Fig. 1a. Throughout successive cycles, an incremental accumulation of plastic strain is observed. Simultaneously, the stress plateaus exhibit increased steepness, and the initially sharp transition from the elastic regime to the plateau becomes more rounded. The stress–strain curve narrows, indicating a reduction in the area enclosed by the trajectory. After 20 cycles, the sample manifests a distinctive cigar-shaped characteristic, having accumulated a plastic strain of 1.5%.

The preceding discussion establishes a pronounced influence of cycle number on the superelastic performance of TiNi film samples. Consequently, a comprehensive analysis of the strain rate dependence on mechanical work input and elastocaloric effect size is conducted on samples that have undergone sufficient cycles to achieve mechanical behavior stabilization. The mechanical work at different strain rates is presented in Fig. 1b. Under adiabatic conditions, the measured mechanical work input is 6.9 MPa, while under isothermal conditions, it is 3.2 MPa. Peak temperatures, depicted as a function of strain rate in Fig. 1c, are determined by averaging the temperature over a designated test area of 1 mm^2 at the sample center using IR thermography. In the adiabatic limit, reached at a strain rate of 0.2 s^{-1}, the temperature change is observed to be 16 K during loading and − 15 K during unloading.

TiNiFe Foils

Ternary foil samples with chemical composition $Ti_{49.1}Ni_{50.5}Fe_{0.4}$ have been prepared by cold rolling with

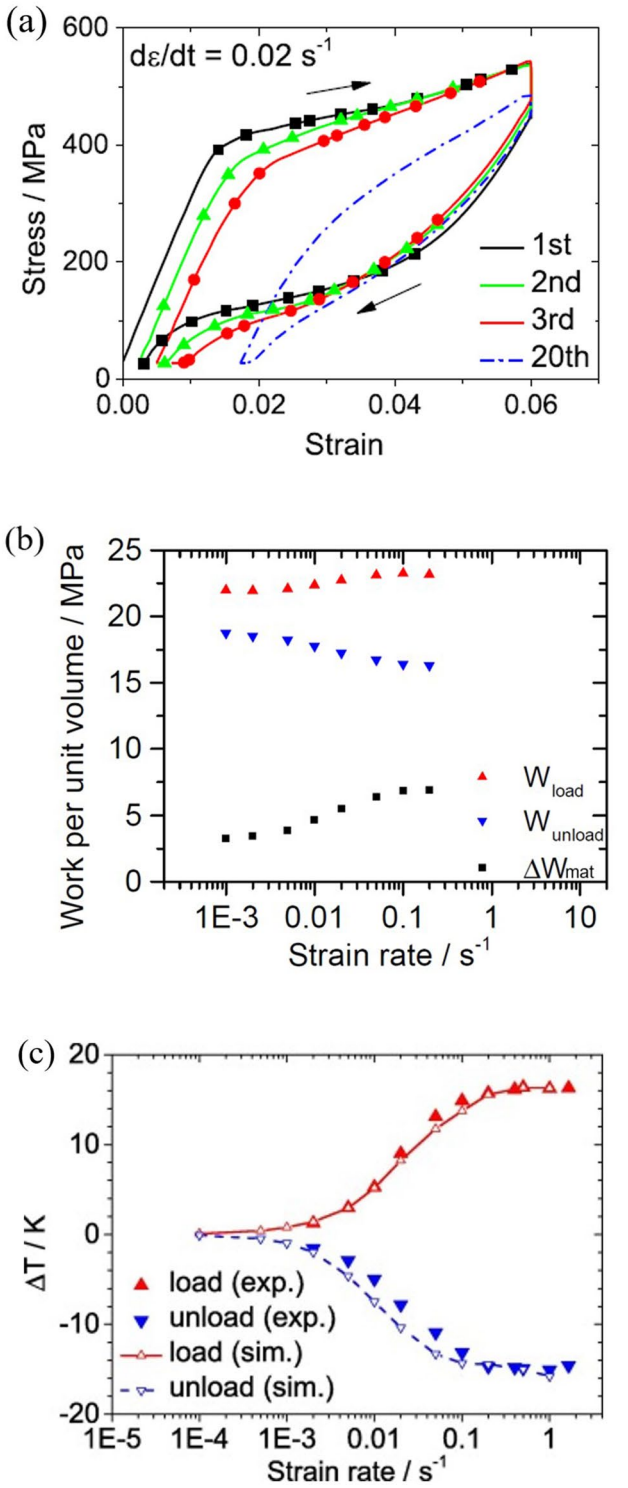

Fig. 1 Thermal–mechanical performance of a $Ti_{49.6}Ni_{50.4}$ film sample: **a** Stress–strain characteristics as a function of cycle number [21]. Reprinted from H. Ossmer et al., Local Evolution of the Elastocaloric Effect in TiNi-Based Films, *Shape Memory and Superelasticity*, Vol *1*, Pages 142–152, Copyright 2015, Springer Nature; **b** Mechanical work W_{load} and W_{unload} for loading and unloading, as well as work input $\Delta W_{mat} = W_{load} - W_{unload}$ as a function of strain rate [22]. Reprinted from *Acta Materialia*, Vol 81, Ossmer, H., Lambrecht, F., Gültig, M., Chluba, C., Quandt, E., & Kohl, M., Evolution of temperature profiles in TiNi films for elastocaloric cooling, Pages 9–20, Copyright 2014, with permission from Elsevier; **c** Peak temperature changes reached during loading as a function of strain rate [22]. Reprinted from *Acta Materialia*, Vol 81, Ossmer, H., Lambrecht, F., Gültig, M., Chluba, C., Quandt, E., & Kohl, M., Evolution of temperature profiles in TiNi films for elastocaloric cooling, Pages 9–20, Copyright 2014, with permission from Elsevier

a final thickness of 30 µm. The final heat treatment has been performed at 450 °C for 30 min. Given the impact of the fabrication process on mechanical performance concerning sample orientation with respect to the rolling direction, tensile tests were executed on samples oriented in both the rolling direction (RD) and transverse direction (TD).

The initial focus is on assessing the dependency of mechanical performance of the sample on the cycle number. Figure 2a illustrates the mechanical performance concerning cycle number in both RD and TD. In both samples, the stress plateau experiences a reduction during loading and unloading as the cycle number increases. Cycle-to-cycle deviation reaches its peak in the initial cycles and progressively decreases over subsequent cycles. For a strain of 3%, within the first 100 cycles, the plateau stress of forward transformation decreases by 10% for TD and 14% for RD loading. Similarly, the reverse transformation plateau experiences a 5% decrease for TD and a 12% decrease for RD. The stabilization cycle number, determined through exponential fits, is approximately 30 cycles. Analyzing the cycle-dependent eC effect size via IR measurements reveals no pronounced impact of training on the peak temperature changes. In Fig. 2b, the mechanical work of loading and unloading, along with the work input (their difference), is depicted as a function of strain rate in the RD. The work input increases with the strain rate until adiabatic conditions are reached at a strain rate of 0.2 s^{-1}. Under adiabatic conditions, the measured mechanical work input is 9.5 MPa, whereas under isothermal conditions, it is 5.4 MPa. In Fig. 2c, the peak temperature changes during loading and unloading at various strain rates are presented. In the adiabatic limit, temperature changes of 20.2 K during loading and − 15.9 K during unloading are observed. Measurements conducted in both RD and TD indicate that the sample's texture orientation plays a minor role in the elastocaloric temperature change.

TiNiCuCo Films

The sputter-deposited TiNi films discussed in the preceding section exhibit a substantial eC effect size. However, the practical application is limited due to pronounced cycle-dependent changes in the eC effect, largely attributed

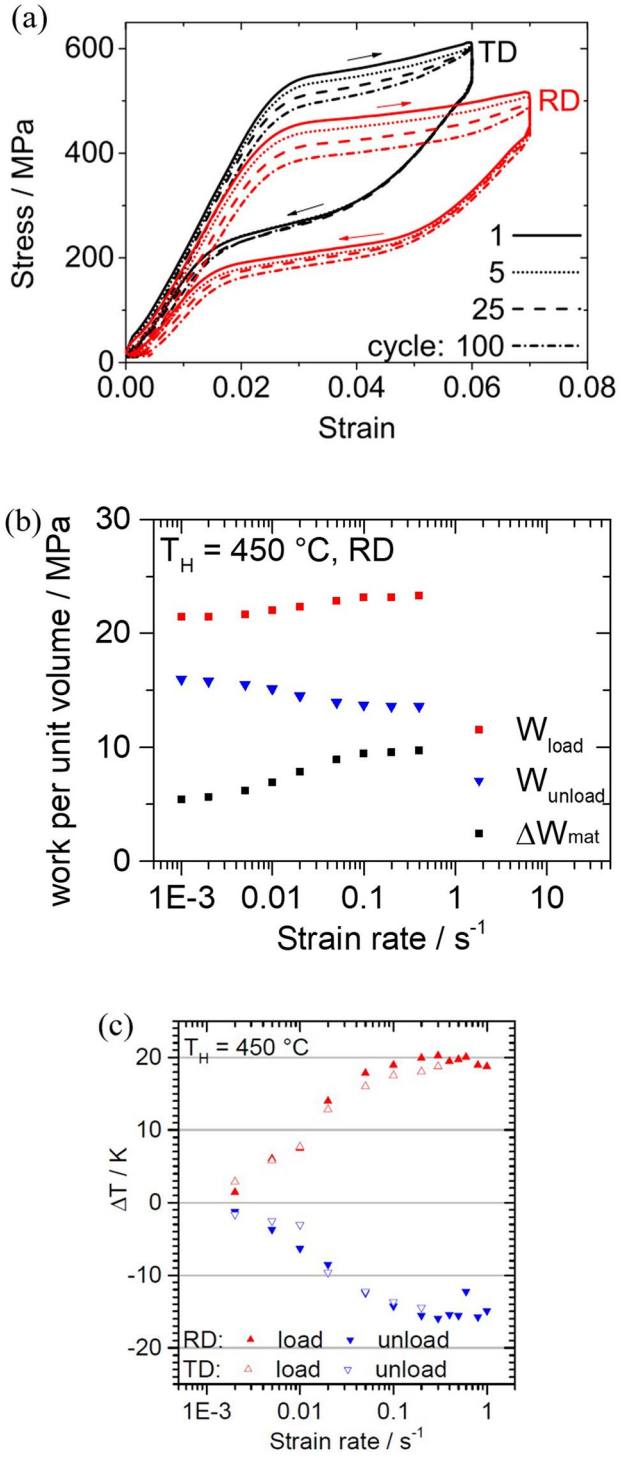

Fig. 2 Thermal–mechanical performance of a $Ti_{49.1}Ni_{50.5}Fe_{0.4}$ foil sample: **a** Stress–strain characteristics as a function of cycle number in rolling direction (RD) and transverse direction (TD) [23]. Used with permission of IOP Publishing, Ltd, from *Smart Materials and Structures*, Ossmer, H., Wendler, F., Gueltig, M., Lambrecht, F., Miyazaki, S., & Kohl, M., *25*(8), 2016; permission conveyed through Copyright Clearance Center, Inc.; **b** Mechanical work W_{load} and W_{unload} for loading and unloading, as well as work input $\Delta W_{mat} = W_{load} - W_{unload}$ as a function of strain rate in RD, reprinted from Ref. [24], **c** Peak temperature changes reached during loading and unloading as a function of strain rate, reprinted from Ref. [24], © 2017 Ossmer, use permitted under Creative Commons Licence (CC BY-SA 3.0 DE)

to significant fatigue [25]. Promising material systems are Ti–rich TiNiCu and TiNiCuCo films showing no fatigue even after 10 million cycles [26]. Detailed investigations of the microstructure showed that the compatibility of austenite and martensite lattices is an important factor [27]. In addition, the small grain size and coherent precipitates favor the high reversibility [27]. The $Ti_{55}Ni_{29.6}Cu_{12.6}Co_{2.8}$ film samples in this study are fabricated by DC magnetron sputtering. The 22 µm thick samples are heat treated by rapid thermal annealing at 700 °C for 15 min to ensure sample homogenization and recrystallization.

Figure 3a shows selected stress–strain characteristics of the first 1000 mechanical load cycles of a TiNiCuCo film [28]. In contrast to TiNi films and TiNiFe foils discussed earlier, TiNiCuCo films exhibit consistently stable material behavior right from the initial loading cycle. In Fig. 3b, the measured mechanical work input under adiabatic conditions is 2.2 MPa, which is reached at a strain rate above 0.2 s^{-1}. In comparison, under isothermal conditions, the mechanical work input is lower at 0.7 MPa. Figure 3c shows peak temperature changes reached during loading as a function of strain rate. Under the adiabatic limit, the temperature change is 9.3 K during loading and − 12.4 K during unloading.

Local Transformation Behavior

The investigation of localized stress-induced phase transformation is conducted through in-situ Digital Image Correlation (DIC) analysis [21, 22]. In Fig. 4a, the local strain is presented within a representative 3×2 mm^2 test area of a TiNiCuCo film sample during loading and unloading. Local strain maps derived from the test area at the center of the film reveal regions of high local strain, predominantly associated with tension-oriented martensite, while regions of low strain are predominantly austenitic. The study identifies stress-induced and reverse phase transformations occurring through the nucleation and propagation of Lüders-like bands characterized by sharp interfaces. These strain bands exhibit an orientation at an angle of 55° with respect to the tensile direction, where both possible inclinations are observed, resulting in strain bands that either intersect or partially overlap [29]. During both reverse and forward transformations, strain bands tend to emerge at nearly identical positions. At lower strain rates, a limited number of individual bands nucleate and propagate, primarily near the areas where the sample is fixed. The localized strain is correlated with a localized temperature distribution, which is associated with the release and absorption of latent heat at the phase front, as depicted in Fig. 4b.The diagrams unveil the occurrence of self-heating during superelastic loading and self-cooling during unloading.

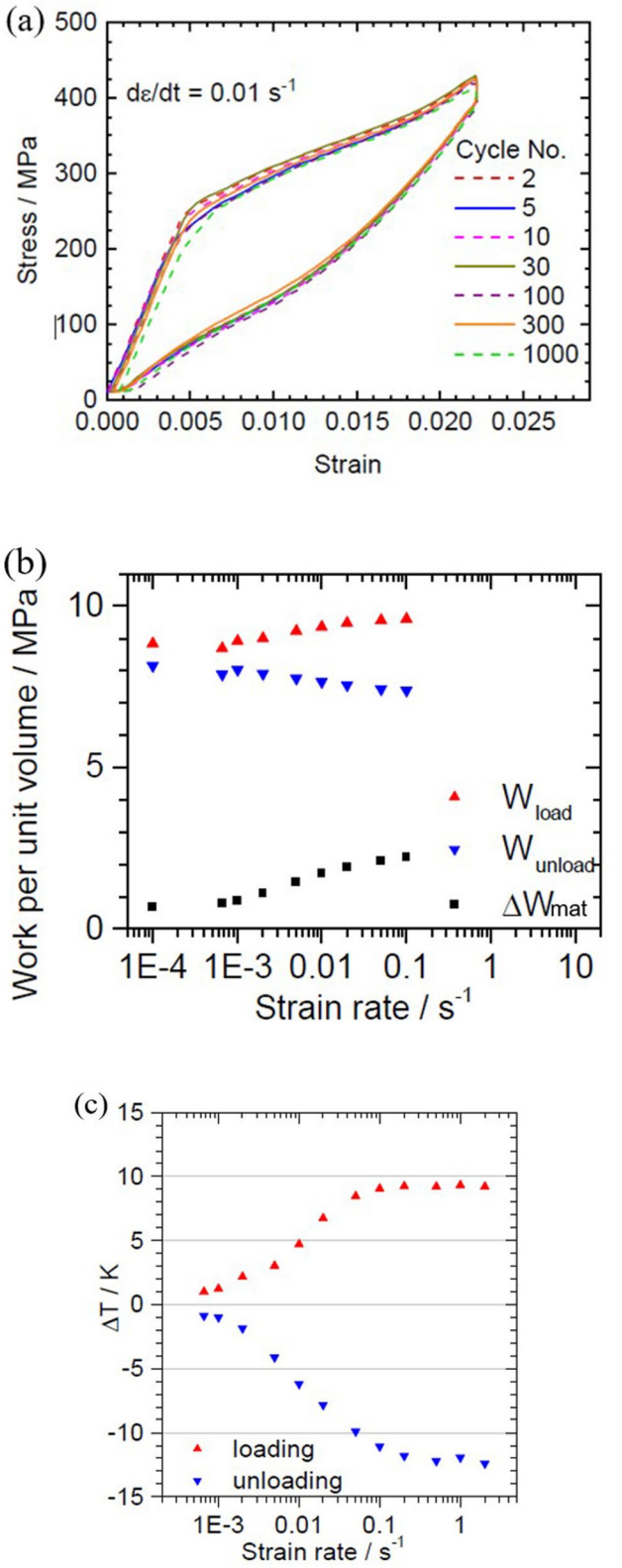

Fig. 3 Thermal–mechanical performance of a $Ti_{55}Ni_{29.6}Cu_{12.6}Co_{2.8}$ film: **a** Stress–strain characteristics as a function of cycle number at a strain rate of 0.01 s^{-1}, reprinted from Ref. [28], © 2020 Brueder-lin, use permitted under Creative Commons Licence (CC BY-SA 4.0). **b** Mechanical work W_{load} and W_{unload} for loading and unloading, as well as work input $\Delta W_{mat} = W_{load} - W_{unload}$ as a function of strain rate, reprinted from Ref. [24], © 2017 Ossmer, use permitted under Creative Commons Licence (CC BY-SA 3.0 DE). **c** Peak temperature changes reached during loading as a function of strain rate, reprinted from Ref. [24], © 2017 Ossmer, use permitted under Creative Commons Licence (CC BY-SA 3.0 DE)

Elastocaloric Properties of SMA Films

The mechanical performance of SMA materials has been investigated under two distinct conditions: the isothermal limit and the adiabatic limit. Isothermal experiments were conducted to determine fundamental material properties such as elastic moduli, Clausius-Clapeyron coefficients, critical stresses, and stress hysteresis, independent of self-heating and cooling effects. However, for practical applications, the more realistic scenario is the adiabatic limit, as high cycling rates are desired to achieve large cooling capacity. Under adiabatic conditions, heat release and absorption occur rapidly, suppressing significant heat transfer to the environment. Consequently, the thermal power primarily results in a temperature change within the elastocaloric material itself.

The mechanical work input, denoted as ΔW_{mat}, representing the amount of work required to drive the elastocaloric cooling cycle once, is depicted by the area enclosed by the stress–strain curve during a load cycle. This work input increases with strain rate and reaches a maximum in the adiabatic limit. Notably, further increases in the strain rate do not lead to a corresponding rise in the work input beyond the adiabatic limit, as the maximum temperature changes have already been reached. An essential parameter, the adiabatic temperature change (ΔT_{ad}), is determined through tensile tests conducted under adiabatic conditions, employing infrared measurements. The latent heat of the transformation (Q_{lat}) is estimated based on ΔT_{ad} and the specific heat capacity of the material (c_p):

$$Q_{lat} = c_p \cdot \Delta T_{ad}$$

To quantify the efficiency of the elastocaloric effect within a material, the material coefficient of performance COP_{mat} is defined

$$COP_{mat} = \frac{Q_{lat}}{\Delta W_{mat}}$$

The eC properties of the investigated TiNi-based films are summarized in Table 1. The values for COP_{mat} for cooling are determined by extracting ΔW_{mat} and Q_{lat} from tensile tests during the unloading process, assuming full recovery of the unloading work. Among the materials studied, sputter-deposited TiNiCuCo films exhibit the highest cooling

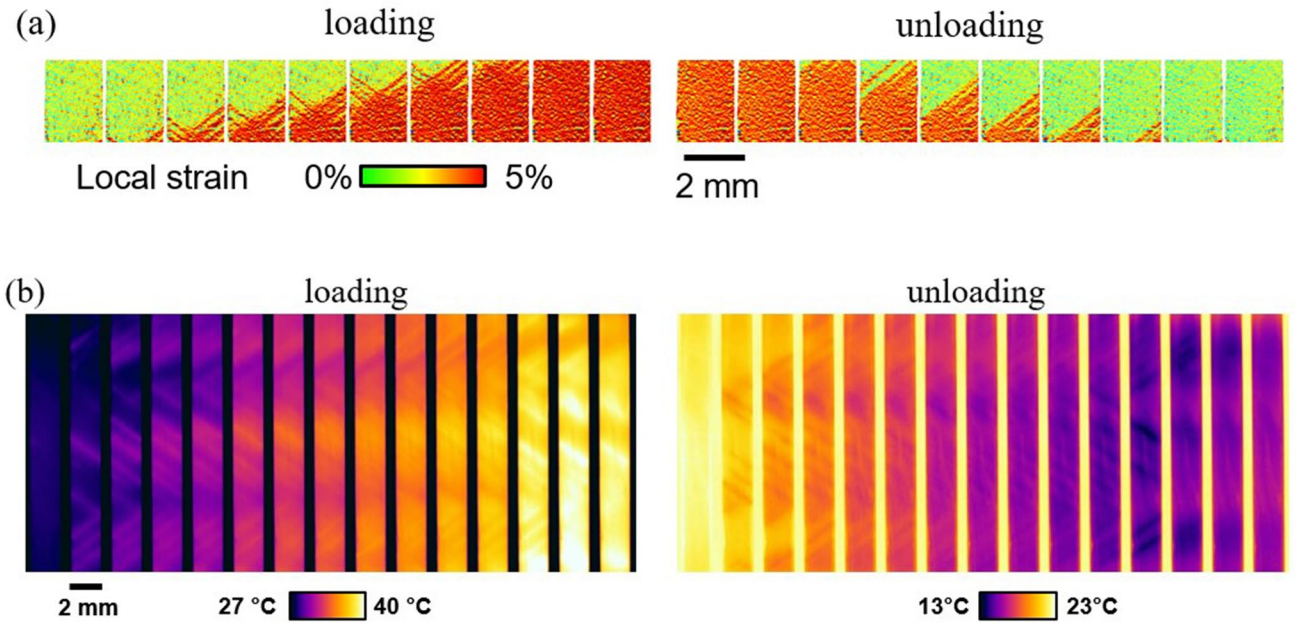

Fig. 4 **a** Local strain and **b** temperature distribution of a TiNiFe film sample during loading and unloading at a strain rate of 0.02 s^{-1}, reprinted from Ref. [24], © 2017 Ossmer, use permitted under Creative Commons Licence (CC BY-SA 3.0 DE)

Table 1 Summary of elastocaloric properties of SMA materials, determined by tensile test and infrared thermography. All measurements are conducted under the trained state of the SMA materials. The COP values provided in the analysis assume full recovery of the unloading work. Critical stress characterization under isothermal conditions involves the tangential method. AM refers to the austenite to martensite phase transformation, while MA denotes reversibility

	$Ti_{49.6}Ni_{50.4}$	$Ti_{49.1}Ni_{50.5}Fe_{0.4}$	$Ti_{55}Ni_{29.6}Cu_{12.6}Co_{2.8}$
Thickness [mm]	0.02	0.03	0.022
AM critical stress [MPa]	500	475	390
MA critical stress [MPa]	410	340	365
Isothermal work input [MPa]	3.2	5.4	0.7
Adiabatic work input [MPa]	6.9	9.5	2.2
Latent heat [J/g]	7.5	8.6	6.25
Adiabatic temperature change (heating) [K]	16.4	20.2	9.3
Adiabatic temperature change (cooling) [K]	− 15.1	− 15.9	− 12.4
COP_{mat} (cooling)	7.7	10.5	14

COP_{mat} of 14, attributed to their notably low hysteresis. While the adiabatic temperature changes in these quaternary films are somewhat lower compared to binary TiNi samples, the advantage lies in their significantly lower hysteresis and ultra-low fatigue. In contrast, sputter-deposited TiNi films achieve a cooling COP_{mat} of up to 7.7. TiNiFe foils have demonstrated cooling COP_{mat} values of up to 10.5.

The functional properties of SMAs can be adjusted through various means, such as additional alloying elements or specific heat treatments. However, in most cases, hysteresis and latent heat cannot be independently tuned within the same material. Consequently, achieving an optimal balance is essential among the elastocaloric effect, mechanical hysteresis, and cyclic stability to ensure effective performance.

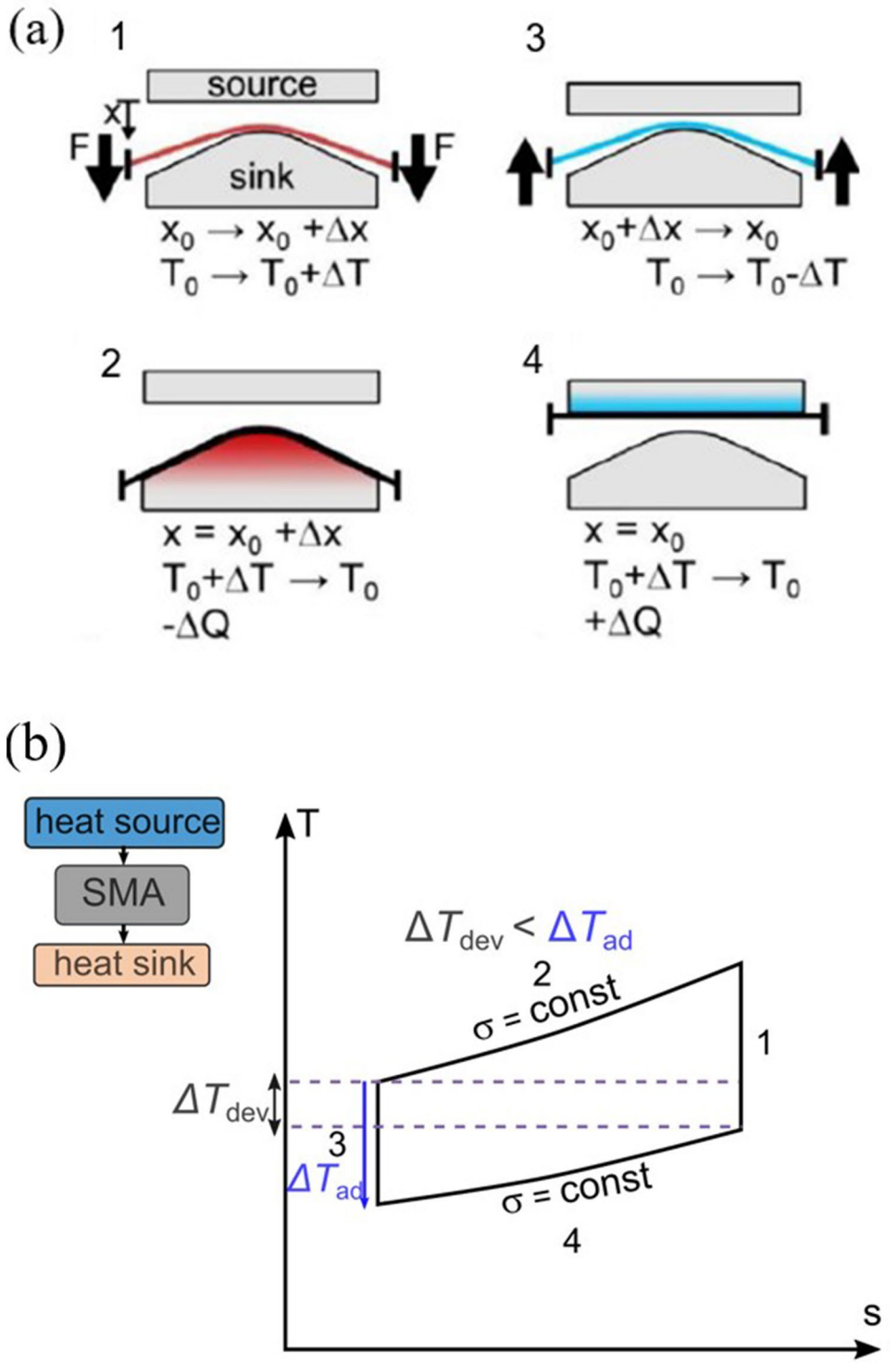

Fig. 5 **a** Single SMA film-based elastocaloric cooling cycle, **b** Corresponding temperature-entropy diagram, adapted from Ref. [30]

Single SMA Film-Based Elastocaloric Cooling Device

Concept

Figure 5a presents a schematic of single SMA film-based eC cycle. The innovative concept is predicated on the cyclic loading of SMA films in out-of-plane direction, solid-to-solid heat transfer from and to the SMA film, and the separation of the hot and cold heat flows by alternating contact conditions [27, 30]. The setup comprises four principal components: a SMA film, a solid heat sink, a solid heat source, and an actuation mechanism, as denoted by the directional arrows. This configuration necessitates only a single actuator

to alternate between contact conditions and to facilitate the cyclic loading of the SMA film.

The heat sink is uniquely designed with a triangular-shaped surface that engages the SMA film through out-of-plane loading. Conversely, the heat source is equipped with a flat surface, allowing the SMA film to make contact in a low-stress state, thus facilitating heat absorption. To operationalize this setup, the SMA film initially moves towards the heat sink and is pressed against it (step 1). This action results in the simultaneous loading of the SMA film and its contact with the heat sink. Consequently, the latent heat of transformation is released heating the SMA film. Heat transfer to the heat sink occurs via mechanical contact (step 2) and is maintained sufficiently long to approach stationary conditions. Subsequently, the SMA film is repositioned in the opposite direction (step 3), releasing the load and triggering the reverse transformation. This process results in the absorption of latent heat within the SMA film, thereby cooling it. The cooled SMA film is then brought into contact with the heat source (step 4), enabling heat absorption. This process is analogous to the reverse Brayton cycle, as illustrated in Fig. 5b. From a thermodynamic perspective, the single film-based eC device exhibits a limited device temperature range, ΔT_{dev}, defined as the temperature difference between the heat sink and source. This range is constrained by the adiabatic temperature span of the SMA film, ΔT_{ad}.

Device Prototype and Experiment Results

Figure 6a shows the schematic and photographic depiction of the single film-based eC device [27, 31]. The spring-like compliant structures, as opposed to more rigid supports, significantly diminish the need for precision in fabrication, alignment, and operation. Furthermore, they are

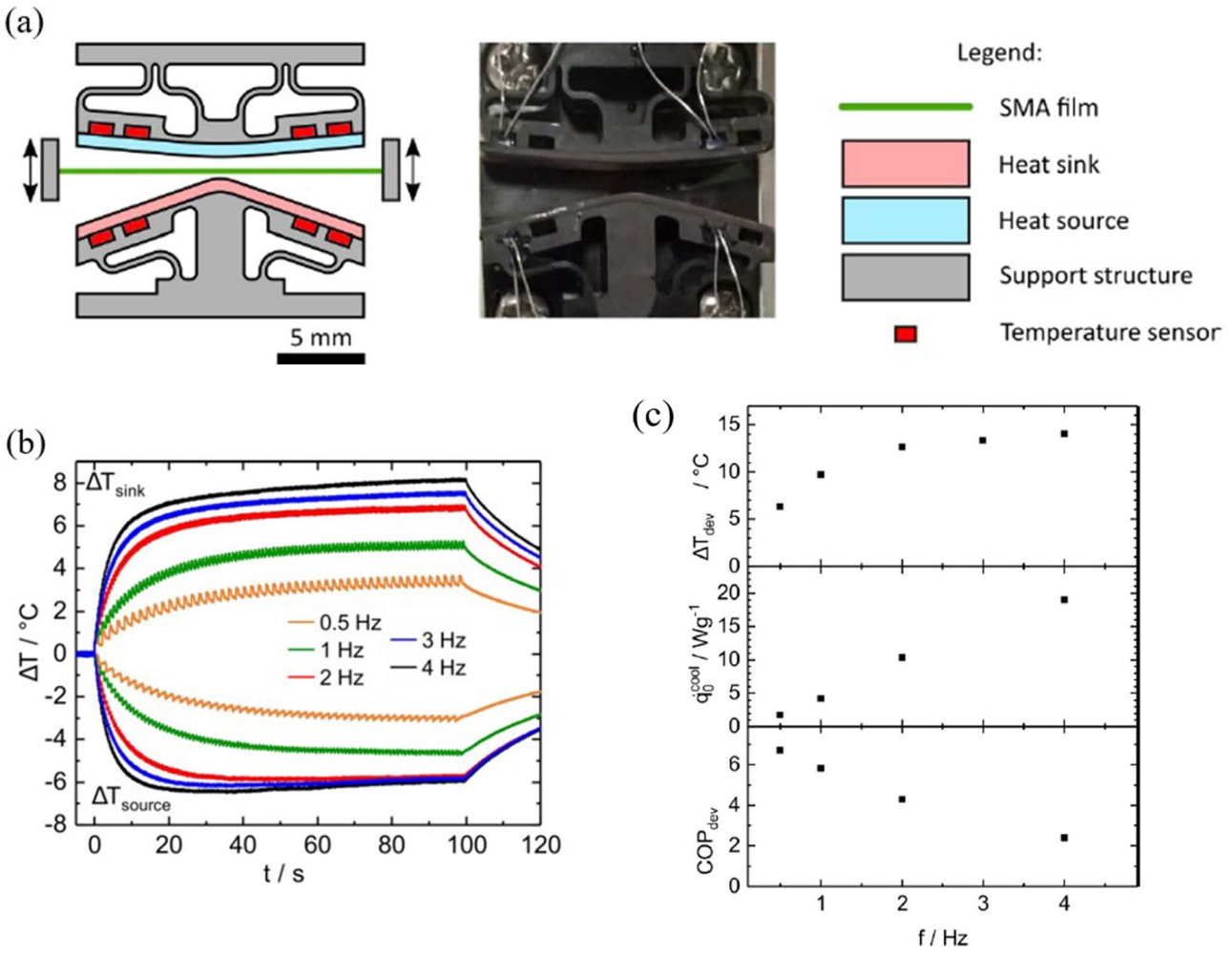

Fig. 6 **a** Schematic setup and photo of the single film-based elastocaloric cooling device, **b** temperature evolution of heat sink and source elements, **c** frequency dependence of device temperature span ΔT_{dev}, specific cooling capacity $\dot{q}_0^{cool}$ and COP_{dev}. Figures reprinted from Ref. [28], © 2020 Bruederlin, use permitted under Creative Commons Licence (CC BY-SA 4.0)

instrumental in ensuring uniform and reproducible mechanical and thermal contact between the SMA film and the copper elements. The heat sink is strategically designed with a 12.7° angle, facilitating a strain of 2.5% on the SMA film when in full contact. The heat source incorporates a slight angle to promote optimal and consistent mechanical and thermal contact. As the active material, a TiNiCuCo film with a thickness of 30 µm is employed. The prototype of the device is fabricated by precision machining for the copper elements and stereolithographic 3D printing for the support structure.

Figure 6b illustrates the temporal evolution of the temperatures of the heat sink and source elements. The plotted data represent the difference between the temperatures of the sink/source and the ambient environment. A range of experiments was conducted at varying operational frequencies, denoted as *f*, ranging from 0.5 to 4 Hz. The observed temperature variations display a stepwise pattern, indicative of the changing contact states between the SMA film and the sink/source elements. At higher operation frequencies *f*, the device exhibits a swifter attainment of saturation and higher temperature changes.

Figure 6c depicts the device's temperature span under saturation (ΔT_{dev}) alongside its specific cooling capacity ($\dot{q}_0^{cool}$) and the COP_{dev}, all as functions of frequency *f*. The ΔT_{dev} escalates with increasing *f* but shows a tendency to saturate, with only marginal increments observed beyond 2 Hz. The maximum ΔT_{dev} achieved is 14 K at 4 Hz, where the maximum $\dot{q}_0^{cool}$ attains a value of 19 W g^{-1}, correlating to an absolute cooling capacity of 220 mW. In terms of efficiency, as measured by COP_{dev}, the peak value of 6.7 is reached at the lowest frequency of 0.5 Hz. The single film-based eC device demonstrates key performance characteristics that establish it as a reference standard within film-based eC devices.

Parallelized SMA Film-Based Elastocaloric Cooling Device

Concept

The reference eC device has demonstrated its efficacy in delivering a large specific cooling capacities of up to 19 W g^{-1}, which translates to an absolute cooling power of about 220 mW per SMA film. To extend the range of potential applications for SMA film-based eC devices, an advanced parallelized approach has been proposed, aimed at enhancing the absolute cooling capacity [27, 31]. This approach, depicted in Fig. 7b, involves the parallel arrangement of SMA films. Through this configuration, the advantageous high surface-to-volume ratio of SMA films is preserved, while simultaneously aggregating their cooling capacities in proportion to the number of SMA films utilized.

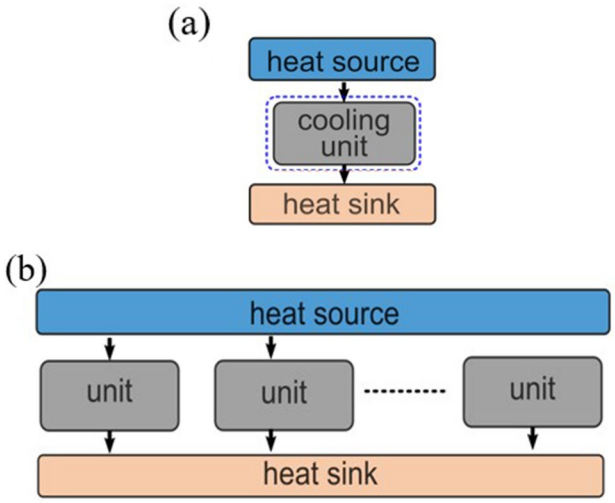

Fig. 7 Concept for enhancement of cooling capacity of SMA film-based eC cooling devices: **a** reference eC device with single SMA film **b** advanced eC device with various SMA films operated in parallel, adapted from Ref. [28]

Device Prototype and Experiment Results

Figure 8a presents both a schematic representation and a photograph of the parallelized film-based eC device. The SMA films in this device are configured antagonistically to enable work recovery, thereby augmenting the overall efficiency. Upon actuation in the positive x-direction, SMA films labeled 1, 3, and 5 are subjected to loading as they are pressed against extrusions A, C, and E. Concurrently, films 2 and 4 are relieved of load and make contact with extrusions B and D. As a result, films 1, 3, and 5 conduct heat to the heat sink, while films 2 and 4 absorb heat from the heat source. With a subsequent movement of the frame in the reverse direction, films 1, 3, and 5 are unburdened and engage with extrusions B, D, and F for heat absorption. Simultaneously, films 2 and 4 are pressed against extrusions C and E, thereby relinquishing heat to the heat sink. This cyclical operation facilitates a continuous heat flow from the heat source to the heat sink, mediated by all SMA films. In this configuration, the contact surfaces for the five SMA films are integrated into a single monolithic element. Thus, the heating and cooling power transferred to the heat sink (A, C, E) and source (B, D) by the five SMA films cumulatively contribute to each operational cycle. The active material employed in this demonstrator device consists of NiTiFe films, each with dimensions of 56 mm in length, 4 mm in width, and a thickness of 30 µm.

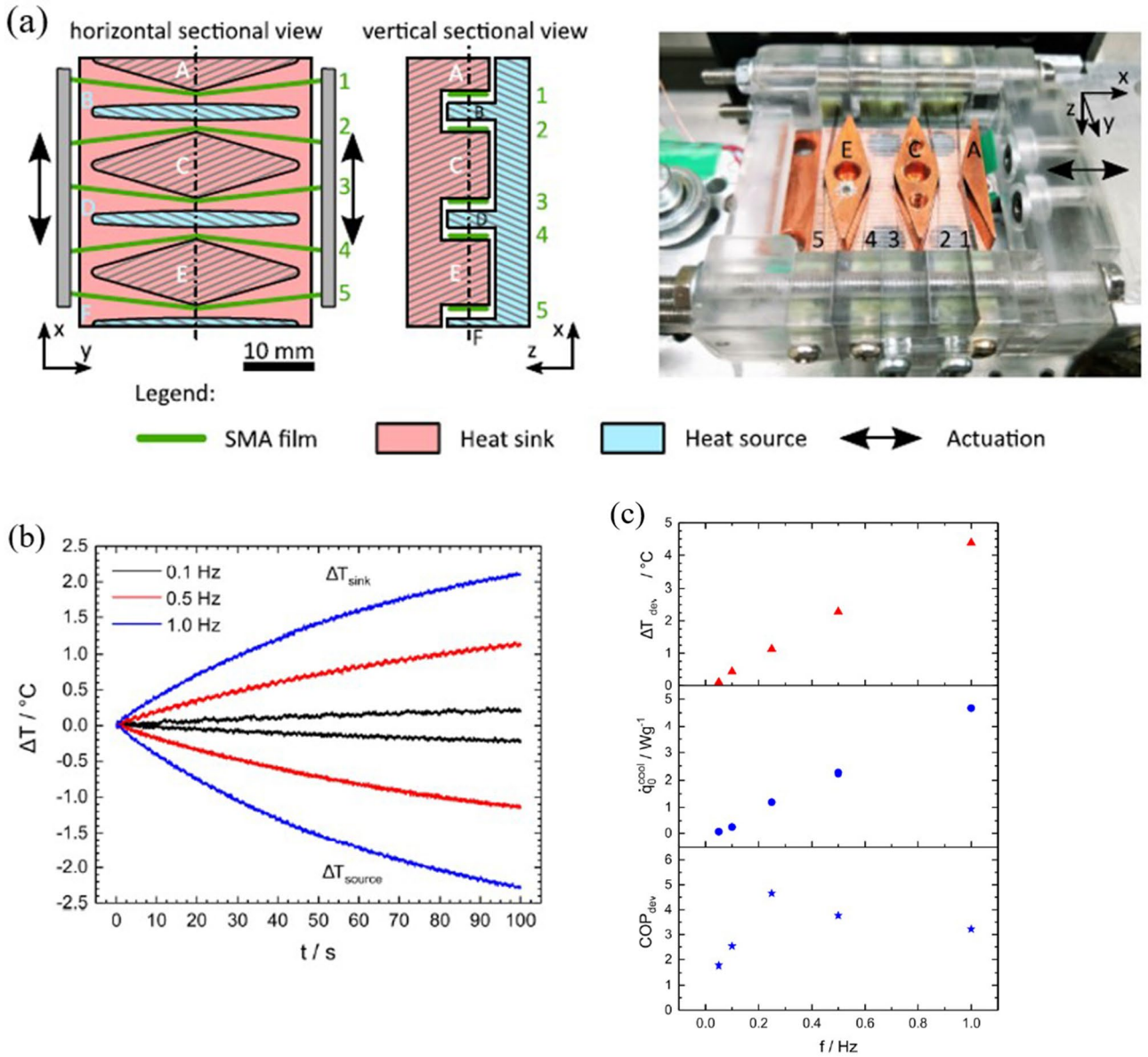

Fig. 8 **a** Schematic setup and photo of the parallelized SMA film-based elastocaloric cooling device. In the photo, the heat source (B, D) is not included to enable the view of the SMA films. **b** Temperature evolution of heat sink and source elements (c) Frequency dependence of device temperature span ΔT_{dev}, specific cooling capacity $\dot{q}_0^{cool}$ and COP_{dev}, reprinted from Ref. [28], © 2020 Bruederlin, use permitted under Creative Commons Licence (CC BY-SA 4.0)

Figure 8b and c present experimental results showing the temperature evolution of the heat sink and source, device temperature span, specific cooling capacity, and COP_{dev} at various frequencies. A maximum ΔT_{dev} of 4.4 K is reached at 1 Hz, lower than the single eC device, likely due to the significantly increased mass of the sink and source elements. The COP_{dev} remains comparable to the single film device, indicating no significant effect of parallelization on efficiency. At 1 Hz, the maximum $\dot{q}_0^{cool}$ is 4.67 W g^{-1}, leading to an absolute cooling capacity ($\dot{Q}_c$) of 0.9 W. Compared to the single film-based eC device at the same frequency, the specific cooling capacity is almost equal for both devices. The absolute cooling capacity of the reference device at 1 Hz is 50 mW, which is increased substantially by a factor of 18 attributed to the combined eC effect of five SMA films and their increased dimensions. However, the potential of higher operation frequencies has not yet been exploited due to experiment restrictions. Further improvements in the experimental device and test platform are expected to reveal the full potential of the parallelized eC cooling setup.

Cascaded SMA Film-Based Elastocaloric Cooling Device

Concept

In the reference eC device, the device temperature span is inherently constrained by the adiabatic temperature change of the SMA film, as depicted in Fig. 5b. To surmount this limitation, a cascaded system architecture, illustrated in Fig. 9a, is proposed [27, 29]. This cascaded system employs a series connection of SMA films, wherein the cooling and heating capacities of one film are utilized to precool or preheat the adjacent film. Consequently, while the temperature span of each individual element remains limited as previously discussed, the cumulative effect in a cascaded arrangement transcends these individual limitations. The operation temperatures of the cascaded elements differ, thereby amplifying the overall temperature span of the system. Figure 9b delineates the temperature-entropy diagram for cascaded SMA films.

Figure 10a displays a photograph of a demonstrator with three NiTiFe films arranged in a cascade. The experimental setup primarily consists of four copper elements, labeled A to D, which serve dual roles as heat sinks and sources. Each of the SMA films measures 32 mm in length, 3 mm in width, and 40 µm in thickness. In this configuration, film 1 and film 3 are directly involved in heat absorption and release from the heat source (A) and to the heat sink (D), respectively. The intermediary copper elements (B and C) act as thermal connectors, simultaneously functioning as a heat sink for one film and a heat source for another. Different from the out-of-plane loading approach, here the SMA films are subjected to in-plane loading, necessitating two actuators: one for loading the SMA films and another for altering the thermal contacts. This arrangement has been chosen to provide enhanced flexibility in adjusting and investigating operational parameters individually, such as maximum applied strain and loading strain. Mechanical compliance in the contact of SMA film and the heat sink and source elements is of high importance for device operation. This is accomplished by making use of the material compliance of an elastomer rather than the structural compliance of a spring. A compliant element made of PDMS is incorporated between the copper elements and the support structure.

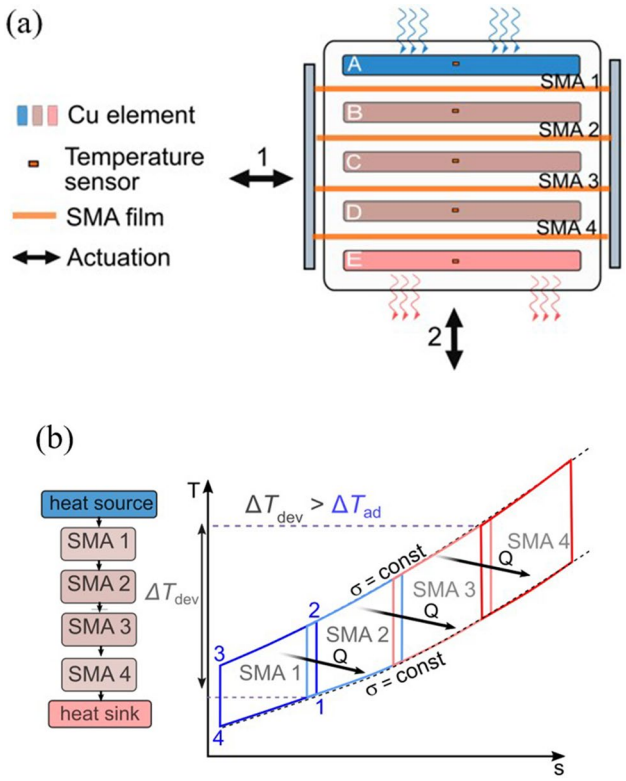

Fig. 9 Concept for enhancement of adiabatic temperature change of SMA film-based eC cooling devices: **a** Schematic of a cascaded architecture comprising three SMA films and four heat sink/source elements. The films are loaded in-plane (1), while the heat sink/source elements are actuated in perpendicular direction (2), (b) corresponding temperature-entropy diagram, adapted from Ref. [28]

Figure 10b illustrates the temperature evolution of copper elements A through D in the cascaded eC device operating at 1 Hz. The experiment yields a cooling capacity of 190 mW, equivalent to 3.4 W g^{-1}, and a COP_{dev} of 1.9. Notably, a temperature differential of approximately 9 K is observed between each pair of adjacent elements (A and B, B and C, C and D). Consequently, the cumulative temperature span of the device at 1 Hz is determined by summing the temperature differences between these neighboring copper elements, resulting in a total ΔT_{dev} of 27.3 K. Cascading of SMA films has a minor effect on the cooling power, while the COP_{dev} decreases with the number of films due to the increase of input work.

Performance Overview of the SMA Film-Based Devices

Table 2 provides a comprehensive overview of the cooling performance metrics for SMA-film-based eC devices. In the reference system, peak performance is observed at an operating frequency of 4 Hz, achieving a maximum device temperature span of 14 K and a cooling capacity of 19 W g^{-1} or 220 mW. This positions the single film device as a benchmark for subsequent advancements in this research. A parallelized device configuration significantly enhances the absolute cooling capacity to 900 mW at same frequency with single device, an 18-fold increase. These results validate the parallelized device architecture as an effective means to augment the absolute cooling capacity, with no fundamental limitations identified against further scaling. The cascade

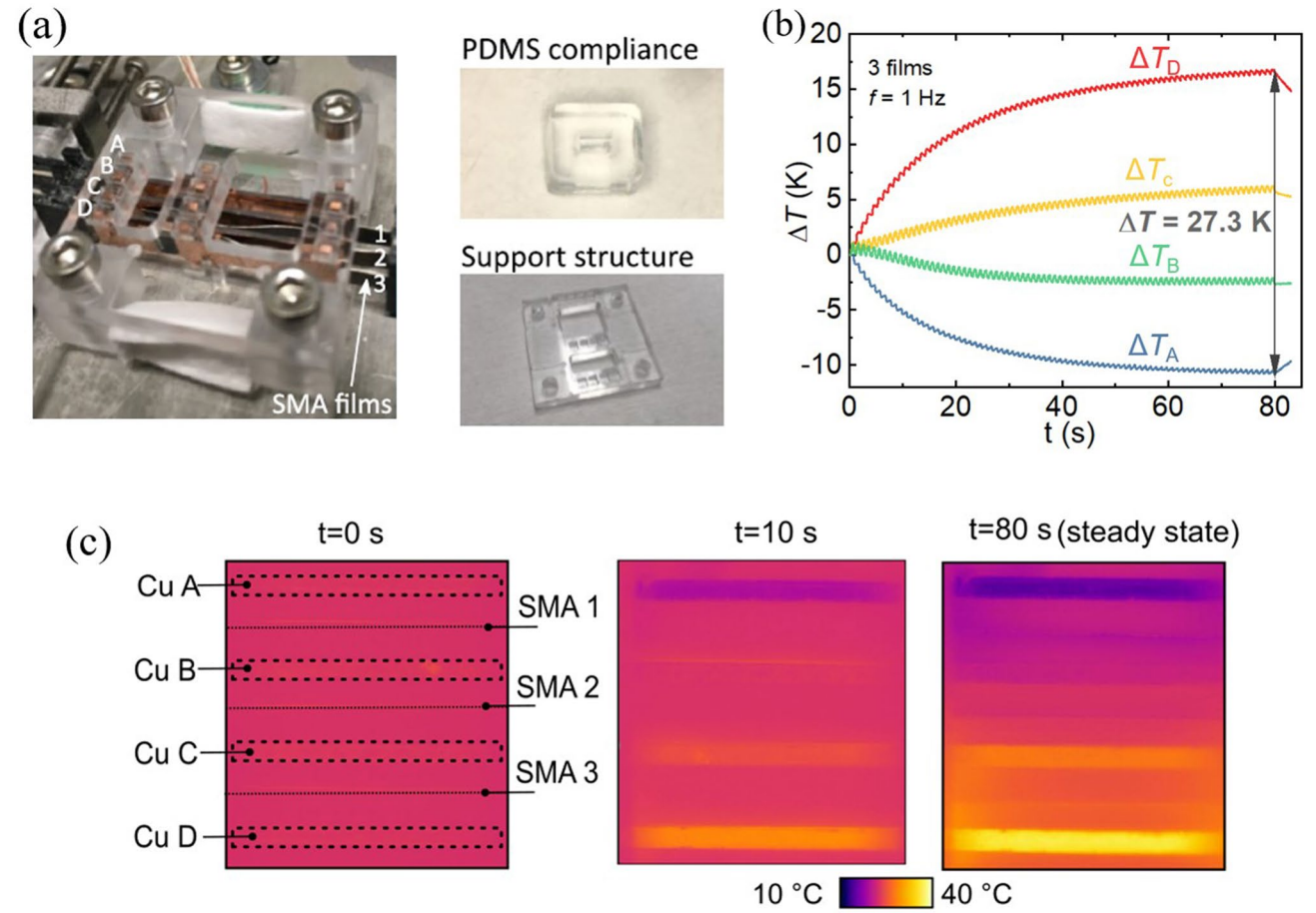

Fig. 10 **a** Photo of the cascaded SMA film-based eC cooling device and components of the device, **b** Temperature evolution of the copper elements A to D of the device at 1 Hz. The temperatures are plotted as temperature difference between the absolute temperature and the initial starting temperature. **c** IR thermographs of the device. Thermographs are taken before, after 10 s, and after 80 s of operation, adapted from Ref. [28]

Table 2 Performance overview of the SMA film-based elastocaloric cooling devices. Indicators: operation frequency f, device temperature span ΔT_{dev}, absolute cooling capacity $\dot{Q}_c$, specific cooling capacity $\dot{q}_0^{cool}$, coefficient of performance COP_{dev}

Device	f [Hz]	ΔT_{dev} [K]	$\dot{Q}_c$[mW]	$\dot{q}_0^{cool}$ [W/g]	COP_{dev}
Single system	0.5	6.3	20	1.7	6.7
	1	9.7	50	4.2	5.8
	2	12.6	121	10.3	4.3
	4	14	220	19	2.4
Parallelized system	0.25	1.1	229	1.2	4.5
	0.5	2.3	436	2.3	3.7
	1	4.4	902	4.7	3.2
Cascaded system					
1 film	1	10.6	168	9	–
2 films	1	21	189	5	–
3 films	1	27.3	193	3.4	1.9

device achieves a maximum temperature span of 27.3 K, more than double the 10.6 K observed in single film devices, through the combined effect of three SMA films. Cascading the elastocaloric effect in a single device is thus proven as an effective strategy for increasing the temperature span. Employing SMA films with tailored transition temperatures, corresponding to varied operational temperature ranges, could further enhance the temperature span of the cascaded device.

The primary challenges in these advanced eC cooling devices (parallelized and cascaded) are the precision and repeatability required in loading the SMA films, impacting both the films' lifespan and the feasible operation frequencies due to heightened demands on actuator precision. Additionally, the likelihood of film failure increases statistically in these advanced systems due to the larger number of films used. Addressing these issues necessitates enhanced fabrication and alignment precision, while reducing precision demands through compliant structures. Moreover, enhancing

the heat transfer between SMA films and heat sink/source could further improve device performance. Potential methods include improving surface quality, adding additional conductive layers, or integrating thermal switches.

In the following, we attempt to compare performance properties of the SMA film-based eC cooling demonstrators with various other macro-scale eC devices. Obviously, such a comparison has to be considered with care, as the devices largely differ by various engineering properties such as the SMA refrigerant in use and the heat transfer concept. Also, the anticipated target requirements might be quite different due to the different application scenarios at miniature and macro scales. Figure 11 offers a comparative analysis of the performance of various reported eC cooling prototypes. The key performance indicators considered are the maximum reported absolute cooling capacity ($\dot{Q}_{c,max}$) at zero temperature span and the maximum reported temperature span ($\Delta T_{dev,max}$) at zero absolute cooling capacity. A comprehensive list of the publications referenced is provided in Table 3. Based on the geometry of SMA materials, eC devices are categorized into several types: films/foil, wires, tubes, and plates. The highest reported $\Delta T_{dev,max}$ and $\dot{Q}_{c,max}$ to date are 50.6 K [14] and 283.9 W [15], respectively. These figures underscore advancements in the active regeneration concept, which employs solid-to-fluid heat transfer between the SMA and the heat sink/source. The figure illustrates that tube-based eC devices exhibit a broader temperature span compared to other SMA material geometries. This is attributed to two factors: first, the utilization of active regeneration [9, 15], composed of parallel SMA tubes of sufficient length, which enhances the regeneration process and leads to a wider temperature span. Second, the use of a tubular SMA regenerator with a spiral cross-section structure [14], offering a larger specific heat transfer area, further contributes to increasing the temperature span. For film-based eC cooling, the simplicity and ease of integration offered by solid-to-solid contact, particularly for electronic components and chips, makes it a viable option for miniature scale.

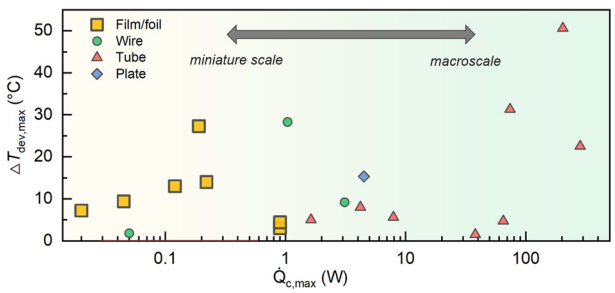

Fig. 11 Comparisons of maximum reported absolute cooling capacity $\dot{Q}_{c,max}$ at zero temperature span and maximum reported temperature span $\Delta T_{dev,max}$ at zero absolute cooling capacity. The corresponding publication list is given in Table 3

Table 3 Performance of reported elastocaloric cooling prototypes. Superscript a is for heating power

References	Material	Geometry	$\Delta T_{dev,max}$ [K]	$\dot{Q}_{c,max}$[W]
[6]	TiNiCuCo	Film/foil	14	0.22
[8]	NiTi	Tube	4.7	65
[9]	NiTi	Tube	31.3	74[a]
[13]	NiTi	Wire	28.3	1.04
[13]	NiTi	Plate	15.3	4.5[a]
[14]	NiTi	Tube	50.6	203.5
[15]	NiTi	Tube	22.5	283.9
[16]	NiTi	Tube	5.6	7.9
[23]	TiNiFe	Film/foil	9.4	0.045
[28]	TiNiFe	Film/foil	27.3	0.19
[32]	TiNiFe	Film/foil	4.4	0.90
[33]	TiNiFe	Film/foil	7	0.02
[34]	NiTi	Tube	1.5	38
[35]	TiNiFe	Film/foil	13.0	0.12
[36]	NiTi	Wire	1.8	0.05
[37]	Rubber	–	7.9	0.877
[38]	NiTi	Tube	5.0	1.63
[39]	Rubber	–	5.2	0.92
[40]	NiTi	Wire	9.2	3.1
[41]	NiTi	Tube	8	4.2

Conclusions

This paper gives an overview on SMA film-based elastocaloric cooling. The need for new innovative cooling technologies that avoid critical substances and provide efficient cooling is constantly increasing in various application fields. The ongoing trend of miniaturization and resulting increased heat flux densities pose severe challenges for today's technology trends and raise the demand for new efficient technologies for cooling and temperature control at small scales. EC cooling is a new solid-state-based technology. It has the potential to provide efficient and environmentally friendly cooling at various scales. The ideal eC material combines a large eC effect size in terms of latent heat of the transformation, isothermal entropy change or adiabatic temperature change with a low work input and therefore high efficiency as well as a high fatigue resistance. In this respect, TiNiCuCo films are of special interest for eC cooling due to their ultra-low fatigue properties and small hysteresis. An eC device has to fulfill several tasks to provide useful cooling and to utilize the promising eC effect. This includes, in particular, cyclic loading of the SMA film(s) to trigger the phase transformation and the related eC effect, transfer of the heat released in the eC material during loading out of the element (hot heat flow) and of the heat absorbed during unloading back into the element (cold heat flow), as well as the separation of the resulting hot and cold heat flows. These tasks are achieved

in film-based eC cooling devices by an oscillating linear actuation and heat transfer via solid–solid contact between SMA film(s) and heat sink/source elements. Owing to the film's large surface-to-volume ratio, this approach proves to be highly suitable for efficient heat transfer avoiding the need of a heat transfer fluid.

The development and characterization of single-stage, parallelized, and cascaded SMA film-based eC demonstrators in this study showcase their versatility and scalability. The single-stage device operated by a single SMA film allows for a 14 K temperature span and a specific cooling capacity of 19 W g^{-1} at 4 Hz, leading to a 220 mW absolute cooling capacity serving as a reference for further advanced SMA film-based eC systems. The parallelized design effectively increased the cooling capacity to 900 mW. The cascaded device, addressing temperature span limitations, attained a temperature span of 27.3 K. This research emphasizes the potential of SMA film-based eC cooling as a sustainable and efficient solution for thermal management in small-scale applications, such as microelectronics and biomedical chips. While there are challenges like precise loading of SMA films and further optimizing heat transfer, future advancements in fabrication and design optimization hold the promise of enhancing the performance and wider applicability of these cooling devices.

Funding Open Access funding enabled and organized by Projekt DEAL.

Data availability Data are available on request.

References

1. Energy Information Administration (EIA) (2019) International energy outlook
2. Vining CB (2009) An inconvenient truth about thermoelectrics. Nat Mater 8(2):83–85
3. Ossmer H, Kohl M (2016) Elastocaloric cooling: stretch to actively cool. Nat Energy 1(10):1–2
4. Wieczorek A, Frenzel J, Schmidt M, Maaß B, Seelecke S, Schütze A, Eggeler G (2017) Optimizing Ni–Ti-based shape memory alloys for ferroic cooling. Funct Mater Lett 10(01):1740001
5. Frenzel J, Wieczorek A, Opahle I, Maaß B, Drautz R, Eggeler G (2015) On the effect of alloy composition on martensite start temperatures and latent heats in Ni–Ti-based shape memory alloys. Acta Mater 90:213–231
6. Bruederlin F, Bumke L, Chluba C, Ossmer H, Quandt E, Kohl M (2018) Elastocaloric cooling on the miniature scale: a review on materials and device engineering. Energ Technol 6(8):1588–1604
7. Cirillo L, Greco A, Masselli C (2024) The energy performances of an elastocaloric device for air conditioning through numerical investigation. Appl Therm Eng 236:121517
8. Qian S, Wang Y, Geng Y, Ling J, Muehlbauer J, Hwang Y, Takeuchi I (2016) Experimental evaluation of compressive elastocaloric cooling system
9. Ahčin Ž, Dall'Olio S, Žerovnik A, Baškovič UŽ, Porenta L, Kabirifar P, Tušek J (2022) High-performance cooling and heat pumping based on fatigue-resistant elastocaloric effect in compression. Joule 6(10):2338–2357
10. Schmidt M, Kirsch SM, Seelecke S, Schütze A (2016) Elastocaloric cooling: from fundamental thermodynamics to solid state air conditioning. Sci Technol Built Environ 22(5):475–488
11. Engelbrecht K, Tušek J, Eriksen D, Lei T, Lee CY, Tušek J, Pryds N (2017) A regenerative elastocaloric device: experimental results. J Phys D Appl Phys 50(42):424006
12. Kirsch SM, Welsch F, Ehl L, Michaelis N, Motzki P, Schütze A, Seelecke S (2019) Continuous operating elastocaloric heating and cooling device: air flow investigation and experimental parameter study. Smart Mater Adapt Struct Intell Syst 59131:V001T04A018
13. Snodgrass R, Erickson D (2019) A multistage elastocaloric refrigerator and heat pump with 28 K temperature span. Sci Rep 9(1):18532
14. Tušek J, Engelbrecht K, Eriksen D, Dall'Olio S, Tušek J, Pryds N (2016) A regenerative elastocaloric heat pump. Nat Energy 1(10):1–6
15. Zhou G, Zhu Y, Yao S, Sun Q (2023) Giant temperature span and cooling power in elastocaloric regenerator. Joule 7(9):2003–2015
16. Qian S, Catalini D, Muehlbauer J, Liu B, Mevada H, Hou H, Takeuchi I (2023) High-performance multimode elastocaloric cooling system. Science 380(6646):722–727
17. Bachmann N, Fitger A, Maier LM, Mahlke A, Schäfer-Welsen O, Koch T, Bartholomé K (2021) Long-term stable compressive elastocaloric cooling system with latent heat transfer. Commun Phys 4(1):194
18. Bartholomé K, Hess T, Winkler M, Mahlke A, König J (2017) New concept for high-efficient cooling systems based on solid-state caloric materials as refrigerant. Energy and thermal management, air conditioning waste heat recovery. Springer, Berlin, pp 178–186
19. Hess T, Maier LM, Bachmann N, Corhan P, Schäfer-Welsen O, Wöllenstein J, Bartholome K (2020) Thermal hysteresis and its impact on the efficiency of first-order caloric materials. J Appl Phys. https://doi.org/10.1063/1.5132897
20. Carmo JP, Silva MF, Ribeiro JF, Wolffenbuttel RF, Alpuim P, Rocha JG, Correia JH (2011) Digitally-controlled array of solid-state microcoolers for use in surgery. Microsyst Technol 17:1283–1291
21. El-Ali J, Perch-Nielsen IR, Poulsen CR, Bang DD, Telleman P, Wolff A (2004) Simulation and experimental validation of a SU-8 based PCR thermocycler chip with integrated heaters and temperature sensor. Sens Actuators, A 110(1–3):3–10
22. Ossmer H, Chluba C, Gueltig M, Quandt E, Kohl M (2015) Local evolution of the elastocaloric effect in TiNi-based films. Shape Memory Superelasticity 1:142–152
23. Ossmer H, Lambrecht F, Gültig M, Chluba C, Quandt E, Kohl M (2014) Evolution of temperature profiles in TiNi films for elastocaloric cooling. Acta Mater 81:9–20
24. Ossmer H, Wendler F, Gueltig M, Lambrecht F, Miyazaki S, Kohl M (2016) Energy-efficient miniature-scale heat pumping based on shape memory alloys. Smart Mater Struct 25(8):085037
25. Ossmer H (2017) Elastocaloric microcooling. Doctoral dissertation, Karlsruher Institut für Technologie (KIT)
26. Bechtold C, Chluba C, Lima de Miranda R, Quandt E (2012) High cyclic stability of the elastocaloric effect in sputtered TiNiCu

shape memory films. Appl Phys Lett. https://doi.org/10.1063/1.4748307
27. Chluba C, Ge W, Lima de Miranda R, Strobel J, Kienle L, Quandt E, Wuttig M (2015) Ultralow-fatigue shape memory alloy films. Science 348(6238):1004–1007
28. Chluba C, Ge W, Dankwort T, Bechtold C, de Miranda RL, Kienle L, Quandt E (2016) Effect of crystallographic compatibility and grain size on the functional fatigue of sputtered TiNiCuCo thin films. Philos Trans R Soc A: Math Phys Eng Sci 374(2074):20150311
29. Bruederlin F (2020) Advanced elastocaloric cooling devices based on shape memory alloy films. Doctoral dissertation, Karlsruher Institut für Technologie (KIT)
30. Wendler F, Ossmer H, Chluba C, Quandt E, Kohl M (2017) Mesoscale simulation of elastocaloric cooling in SMA films. Acta Mater 136:105–117
31. Bruederlin F, Bumke L, Quandt E, Kohl M (2019) Cascaded SMA-film based elastocaloric cooling. IEEE Xplore. https://doi.org/10.1109/TRANSDUCERS.2019.8808605
32. Ulpiani G, Bruederlin F, Weidemann R, Ranzi G, Santamouris M, Kohl M (2020) Upscaling of SMA film-based elastocaloric cooling. Appl Therm Eng 180:115867
33. Ossmer H, Miyazaki S, Kohl M (2015) Elastocaloric heat pumping using a shape memory alloy foil device. In: 2015 Transducers-2015 18th international conference on solid-state sensors, actuators and microsystems (Transducers). IEEE, pp. 726–729
34. Qian S, Wu Y, Ling J, Muehlbauer J, Hwang Y, Takeuchi I, Radermacher R (2015) Design, development and testing of a compressive thermoelastic cooling prototype. In: International congress of refrigeration
35. Bruederlin F, Ossmer H, Wendler F, Miyazaki S, Kohl M (2017) SMA foil-based elastocaloric cooling: from material behavior to device engineering. J Phys D Appl Phys 50(42):424003
36. Sharar DJ, Radice J, Warzoha R, Hanrahan B, Chang B (2018) First demonstration of a bending-mode elastocaloric cooling 'loop'. In: 2018 17th IEEE intersociety conference on thermal and thermomechanical phenomena in electronic systems (ITherm). IEEE, pp. 218–226
37. Greibich F, Schwödiauer R, Mao G, Wirthl D, Drack M, Baumgartner R, Kaltenbrunner M (2021) Elastocaloric heat pump with specific cooling power of 209 W g^{-1} exploiting snap-through instability and strain-induced crystallization. Nat Energy 6(3):260–267
38. Ianniciello L, Bartholome K, Fitger A, Engelbrecht K (2022) Long life elastocaloric regenerator operating under compression. Appl Therm Eng 202:117838
39. Zhang S, Yang Q, Li C, Fu Y, Zhang H, Ye Z, Wang Q (2022) Solid-state cooling by elastocaloric polymer with uniform chain-lengths. Nat Commun 13(1):9
40. Chen Y, Wang Y, Sun W, Qian S, Liu J (2022) A compact elastocaloric refrigerator. Innovation 3(2):100205
41. Zhang J, Zhu Y, Cheng S, Yao S, Sun Q (2022) Enhancing cooling performance of NiTi elastocaloric tube refrigerant via internal grooving. Appl Therm Eng 213:118657